Proceedings of Engineering and Technology Innovation, vol. 26, 2024, pp. 55-71

Evolution of Vortex Structures Generated by a Rigid Flapping Wing with a Winglet in Quiescent Water

Srikanth Goli[1,*], Arnab Roy[2], Subhransu Roy[3], Imil Hamda Imran[1]

[1]Applied Research Center for Metrology, Standards and Testing (ARC-MST), Research Institute, King Fahd University of Petroleum and Minerals, Dhahran, Saudi Arabia

[2]Aerospace Engineering; [3]Mechanical Engineering, Indian Institute of Technology Kharagpur, Kharagpur, India

Received 13 September 2023; received in revised form 14 November 2023; accepted 15 November 2023

DOI: https://doi.org/10.46604/peti.2023.12838

Abstract

This study aims to the utilization of vortex structures generated through wing flapping for achieving sustainable flight, and the motivation is elicited by the phenomenon observed in natural flyers. The vortex structures in the flow field generated by a flapping rigid wing are captured using vorticity and the LAMDA2 criterion. The study investigates a comparative analysis between a wing both with and without a winglet. Moreover, the influence of flapping frequency is examined as well. For the experiments, particle image velocimetry (PIV) measurements are employed for the flow field around mechanical flapping motion in a quiescent water condition. The flapping mechanism has one-degree freedom, showing a 1:3 ratio in motion, and tested wings at 1.5 and 2.0 Hz. A "modified" vortex filamentation and fragmentation phenomenon is proposed as a significant finding in the present study, based on a comprehensive analysis of the flow field around the wing with a winglet.

Keywords: natural flyers, mechanical flapping, flapping wing, winglet, vortex structures

1. Introduction

Birds like hawks have feathers at the wingtip, which are called winglets. These winglets are being applied in commercial aircraft to reduce power consumption. Therefore, the deployment of the wing with a winglet in mechanical flapping motion may result in a favorable effect of reducing power requirements and would be useful in developing practical flying vehicles. The pros and cons of using winglets were evaluated, and the non-planar configuration wings for fixed-wing aircraft were detailed in [1-8]. The concept of winglet in fixed wing configuration was initiated by Whitcomb [1] and Flechner et al. [2] in the 1970s, and Goli et al. [9] initiated the study of winglet in flapping wing configuration. In nature, the spreading of feathers (winglets) both horizontally and vertically is undertaken by most birds to decrease induced drag through the reduction of kinetic energy retained within the vortex sheets formed in their wake [10]. The reduction of induced drag would lead to lower power consumption in flight [5-6]. Hence, to develop flapping wing vehicles with higher efficiency and consequently lower power requirements, the addition of winglets as appendages to the main wing may be beneficial.

To pursue an efficient flapping configuration design, the thorough examination of vortices encircling the compromising flapping wings emerges as of significance. Concerning the current investigation, the flow field generated was observed to exhibit vortex structures, which were subsequently contrasted between configurations involving a rigid flapping wing accompanied by a winglet and configurations lacking such winglets. The discernment of vortex structures was facilitated through the application of vorticity and the LAMDA2 (λ_2) criterion. The present study has been conducted employing the one degree of freedom (1-DOF) or 1-DOF flapping kinematics. A similar degree of freedom flapping motion kinematics was also

* Corresponding author. E-mail address: srikanth.goli@kfupm.edu.sa

English language proofreader: Chih-Wei Chang

discussed in previous studies [11-15]. The development of miniature flapping vehicles could benefit from the utilization of a kinematics approach based on 1-DOF flapping motion. This choice enables a better understanding of the complex unsteady flow field surrounding the wing, which is responsible for generating the necessary forces to sustain flight. It has been noted by Kato and Kamimura [16] that the flapping mechanism of butterflies, despite being a multi-body system, can be regarded as possessing 1-DOF.

Additionally, this mechanism proves advantageous as it requires minimal linkages and cranks, simplifying its construction and reducing the total weight of the flying vehicle. The optimization of weight is consistently a crucial consideration in practical flying vehicles [17-18]. Some of the recent studies providing future research prospects are discussed as follows. In a computational fluid dynamics study [19], the effects of incorporating winglets into flapping hydrofoils and their impact on wave glider propulsive performance were investigated. Simulation results indicated the addition of winglets reduced tip vortices, improved propulsion efficiency, and enhanced the thrust coefficient.

Another study [20] explored the discrete vortex model (DVM) scheme through numerical simulations, exhibiting the effectiveness of asymmetric flapping in generating lift. Furthermore, it also examined the influence of wing flexibility and the addition of winglets, accentuating the importance of varying wing length during the upstroke for enhanced lift generation. Additionally, a study involving a flapping wing model with two-jointed arms in a wind tunnel experiment [21] revealed the influence of the flapping motion on vorticity concentration, vortex characteristics, and circulation of wingtip vortices. These vortices exhibited a wave-like trajectory and distinctive motion patterns, in contrast to fixed-wing vortices. Proper orthogonal decomposition revealed the formation of vortices through flapping motion and the contribution to the energy to suggest potential applications in vortex control and drag reduction in aircraft wing design.

The justification for the current research is discussed as follows. A typical phenomenon observed in animal flight is the presence of asymmetry angles in flapping strokes, which lead to an asymmetry in the forces needed to attain satisfactory flight. In this study, a 1-DOF flapping motion is deployed, featuring a 3:1 angular asymmetry between the upper half stroke and the lower half stroke. Natural flyers encounter minimal changes in wing aspect ratio during biological growth due to sustaining flight with minor changes in flapping frequency and asymmetric motion to retain high maneuverability and aerodynamic efficiency.

Detailed study of flow features and their sensitivity to minor geometric and kinematic changes, albeit on a simplified model, would enable one to better understand and mimic flying animals when being compared with a particular natural flyer species belonging to different age groups. The natural flyers attest to the undisputable fact, i.e., enjoy the advantage of multiple degrees of freedom flapping motion and possess more complex flexible wing planforms depending on the type of species. Therefore, they would fly much more effectively than any existing mechanical flyers through very efficient dynamic control of their wings.

To the best of the authors knowledge, the concept of winglet in mechanical flapping motion has been introduced by Goli et al. [9], while the flow phenomena around the rigid flapping wing without winglet as vortex filamentation and fragmentation has been proposed in Goli et al. [17, 22]. This study extends this understanding by introducing a related phenomenon, which is termed “modified vortex filamentation and fragmentation.” This concept is developed by investigating the impact of winglets on the flapping motion of a rigid wing.

2. Experimental System

Currently, a 1-DOF flapping motion (Fig. 1(a)) with a four-bar mechanism configuration is deployed, and the dimensions can be found in Goli et al. [11, 17]. The wings, composed of 1.5 mm thick Perspex® acrylic, are manufactured in the form of a flat plate. Fig. 1(b) schematically presents a winglet. Table 1 presents the wing dimensions and operational characteristics.

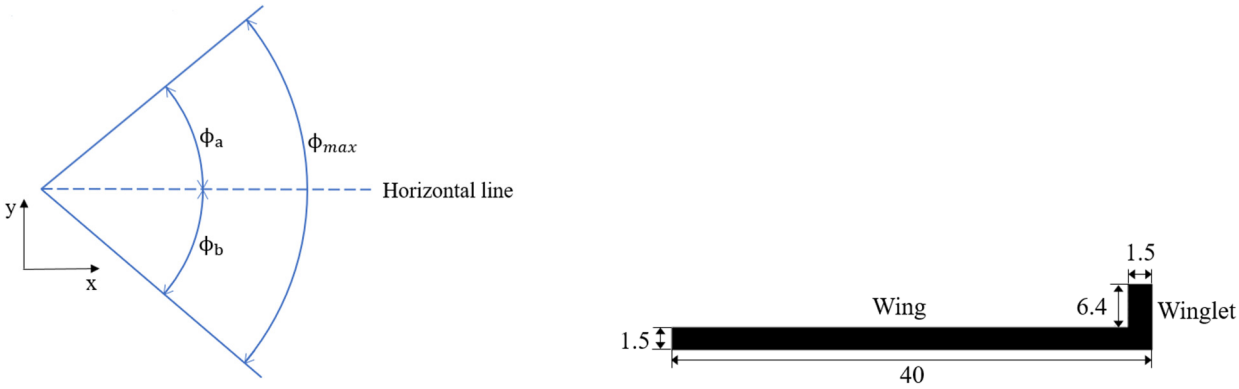

(a) Flapping motion (b) Wing with a winglet (units in mm)

Fig. 1 Schematic view

Table 1 Wing specifications and operating conditions

Case	Span (mm)	Chord (mm)	Thickness (mm)	AR	f (Hz)	Winglet attached	ϕ_a (degree)	ϕ_b (degree)
I-W	40	40	1.5	1.0	1.5	yes	59.5	-14.5
I	40	40	1.5	1.0	1.5	no	59.5	-14.5
II-W	40	40	1.5	1.0	2.0	yes	59.5	-14.5
II	40	40	1.5	1.0	2.0	no	59.5	-14.5

In Fig. 2, the flapping mechanism was mounted on a test stand and fully immersed in the water tank with the free surface of the water exposed to the atmosphere. The fluid was initially maintained in a quiescent condition. Flow field data along the wingspan direction is collected through particle image velocimetry (PIV) measurements by illuminating the wing mid-chord. The primary motivation for using water was to take advantage of improved PIV imaging quality with a more homogeneous dispersion of seeding particles in water [17, 23].

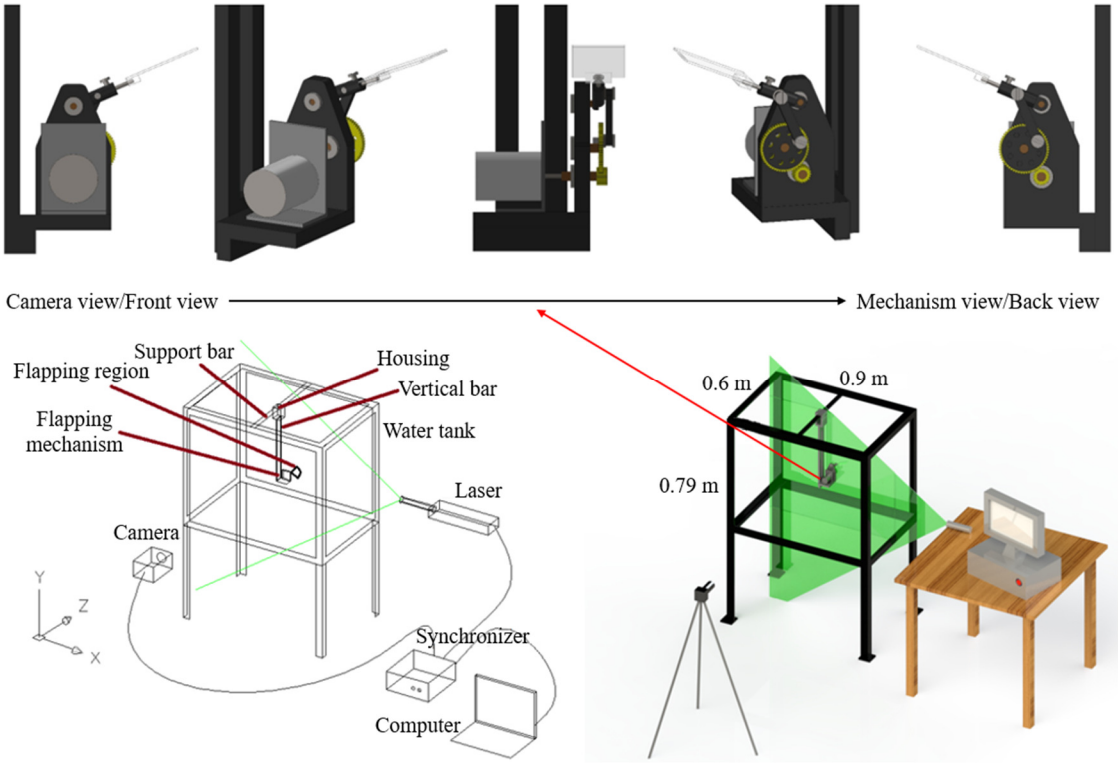

Fig. 2 Experimental setup [9, 22]

Furthermore, the experimental setup for the current work was designed to minimize interference from the sidewalls of the water tank or free surface sloshing effects on the flow around the flapping wing and its surroundings. Thus, the flapping mechanism had to be fully immersed inside the water tank, which was equipped with the walls and free surfaces at sufficiently

large distances to prevent perturbations from boundary proximity effects (details are mentioned below). The incident and reflected perturbations at the side walls and free surface were analyzed over a large number of wing flapping cycles using PIV images and were found to be of negligible order.

The water was seeded with hollow glass particles with a mean diameter of 10 mm and a density of 1.1 g/cc. The percentage of seeding particles was approximately 10^5 (40 ml of water laden with particles mixed with 426 liters of clean water). The PIV measurements were conducted after a continuous 10-minute uninterrupted wing flapping, enabling the flow to reach a periodic state of unsteadiness, ensuring statistically stationary flow field data. Similar tests were reported in Goli et al. [17]. The tests were carried out by illuminating the flow along the span of the wing, with the laser sheet aligned to the mid-chord position of the wing. Besides, the details were reported in Goli et al. [17]. At each discrete flapping angle (ϕ), three instantaneous velocity vector fields were obtained, and the mean of these fields was calculated to determine the phase-locked average velocity vector field. All flow field analysis was based on the average velocity field.

The PIV system consisted of an Nd:YAG dual-pulsed laser with a maximum energy per pulse of 150 mJ, a wavelength of 1064 nm, a laser pulse rate of 14.5 Hz, and a laser thickness of 1.5 mm. The double shutter CCD camera that was used to capture the images had a resolution of 1600 × 1192 pixels at 32 fps. Meanwhile, TSI INSIGHT 3G^{TM} software was employed to process the captured images using a cross-correlation technique with varying interrogation window sizes, 50% overlapping, and time delays of 400 and 350 μs between two frames for flapping frequencies of 1.5 and 2.0 Hz, respectively.

The Nyquist method was used for grid generation, dividing the input images into smaller spots for processing. A Gaussian spot masking algorithm was deployed to condition the spots. fast Fourier transform (FFT)-based correlation functions and Gaussian peak equations were employed for correlation mapping and peak identification, respectively. The collected velocity vectors were interpolated into grids of approximately 3.2 × 3.2 mm^2 to produce one vector. Concerning the processed images, they yielded 12,938 vectors in the view of the flow field for a 1600 × 1192 pixel resolution. The entire study was based on a 24 × 24 interrogation window. The rationale behind this window size is explicated in Goli et al. [17].

The experiments were carried out in a water tank with the free surface of the water exposed to the atmosphere. Insignificant wave motion was observed at the free surface, and negligible effects on the side walls of the tank were recorded through PIV measurements when the flapping mechanism was in operation. Thus, boundary effects did not significantly impact the flow features around the wing. It's noteworthy that the lateral Perspex walls were situated at a distance of 22.5 times the wing span, and the free surface of the water was located at a distance of 19.75 times the wing span. The wingtip peak-to-peak displacement was measured at 108.54 mm, calculated based on the achieved flapping amplitudes.

A similar ratio of peak-to-peak displacement with the water tank was mentioned in Ozen and Rockwell [24]. Uncertainties related to the fabrication and the flapping mechanism were referred to in Goli et al. [17]. In the PIV images, the laser light reflection from the wing section, which affected the intensity in its proximity, was suitably adjusted to match the average background intensity using a Gaussian Kernel filter. After processing the data, spurious vectors accounted for less than 4% of the data from the TSI Insight 3G software, and local medians with a 3 × 3 neighborhood size were used to replace them through interpolation.

3. Results and Discussion

In Section 3.1, the examination of vortex structures for Case I-W and Case I emphasizes significant distinctions between a wing with and without a winglet, at the frequency of 1.5 Hz. Section 3.2 presents a thorough investigation, providing comprehensive details of flow field behavior at two distinct frequencies (1.5 and 2.0 Hz). This examination focuses on the comparison of velocity fields and vorticity with λ_2 criterion to reveal the similarities and dissimilarities in the flow characteristics.

3.1. Comparison of vortex structures for wing with and without a winglet at f =1.5 Hz (Case I-W and Case I)

The vorticity and LAMDA2 (λ_2) distribution for Case I-W (with a winglet) and Case I (without a winglet) at flapping frequency f = 1.5 Hz are depicted in Figs. 3 and 4, while the vorticity and $\lambda_2$criterion are superimposed to capture the vortex structures.

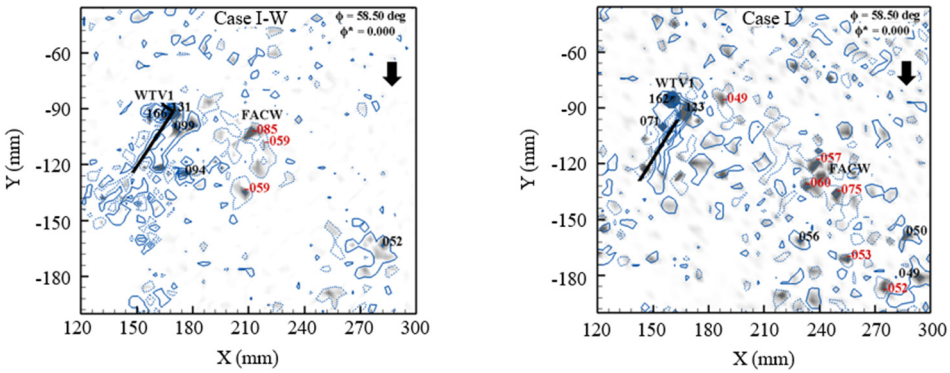

(a) Case I-W and Case I at ϕ = 58.50°

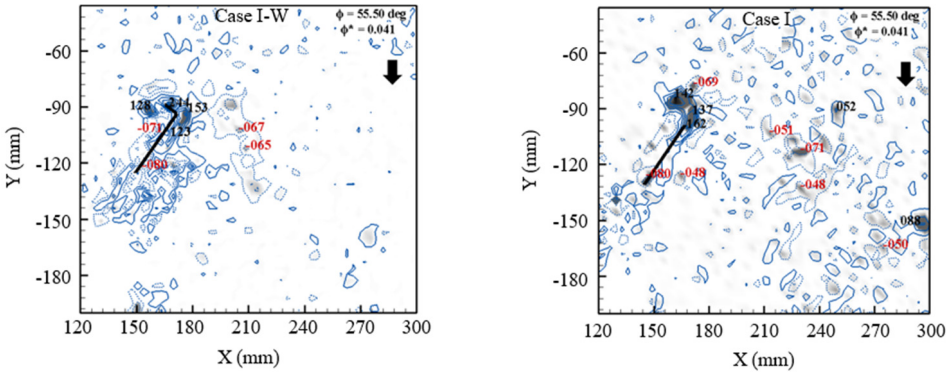

(b) Case I-W and Case I at ϕ = 55.50°

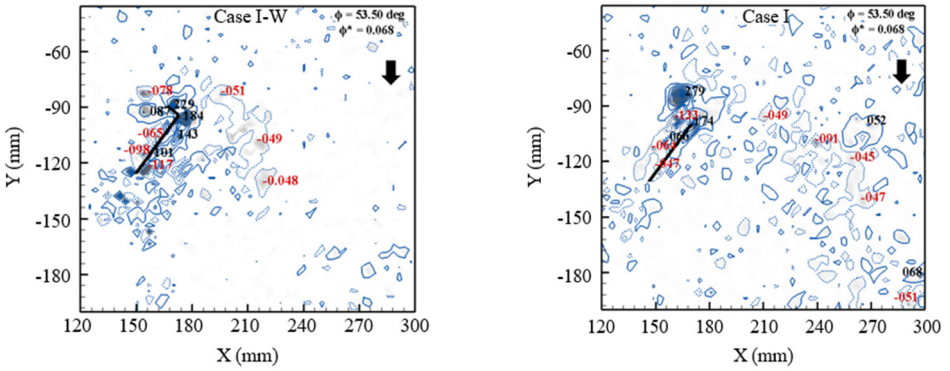

(c) Case I-W and Case I at ϕ = 53.50°

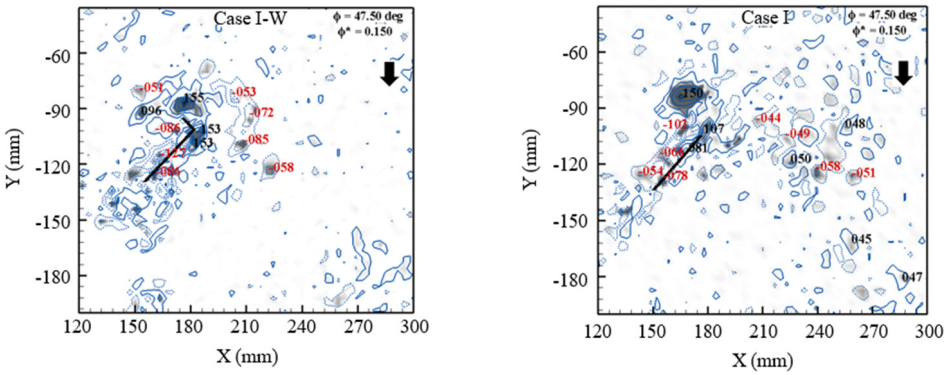

(d) Case I-W and Case I at ϕ = 47.50°

Fig. 3 Evolution of vortex structures during the downstroke of the flapping cycle for Case I-W and Case I at f =1.5 Hz (vorticity- line contour and λ_2 criterion- flood contour)

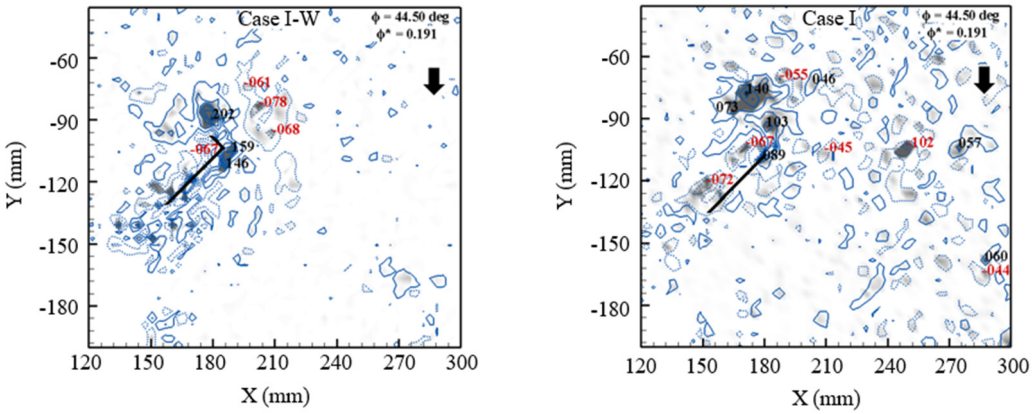

(e) Case I-W and Case I at ϕ = 44.50°

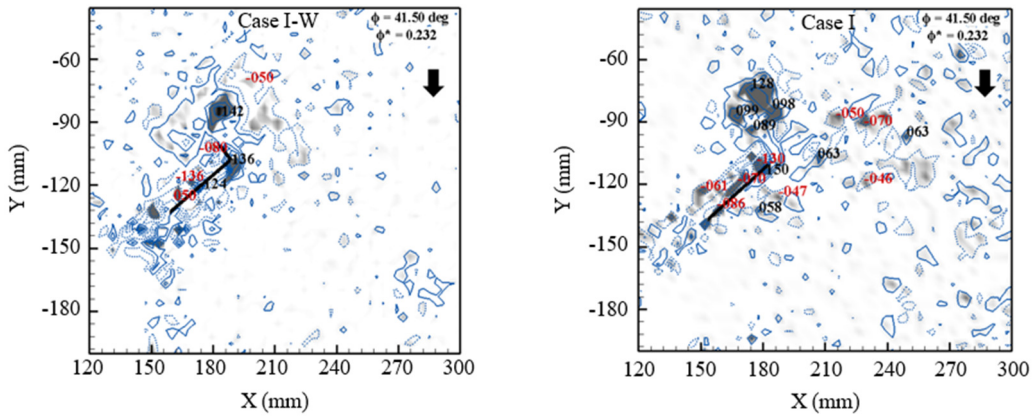

(f) Case I-W and Case I at ϕ = 41.50°

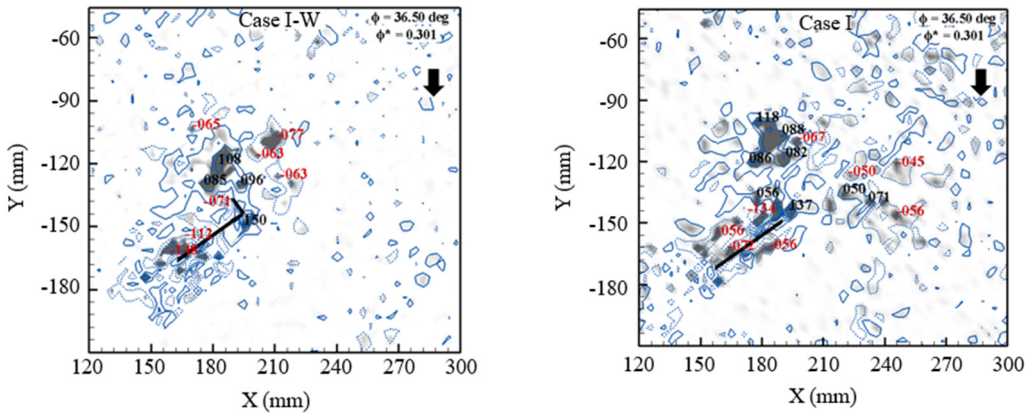

(g) Case I-W and Case I at ϕ = 36.50°

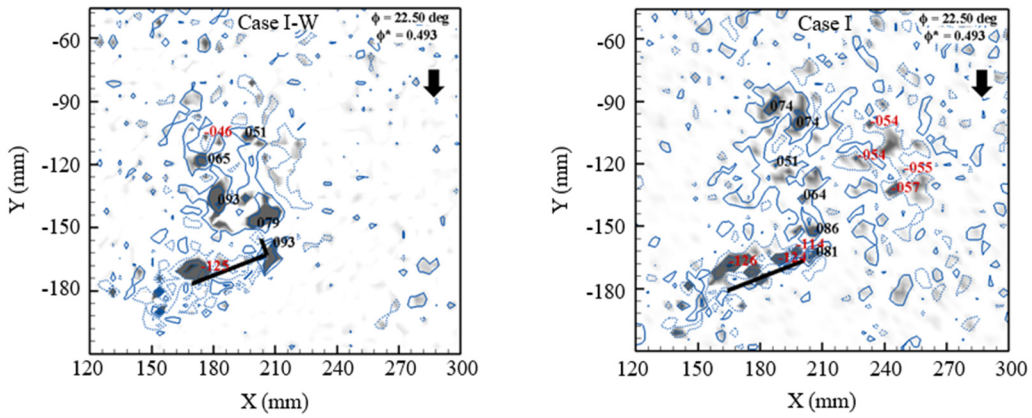

(h) Case I-W and Case I at ϕ = 22.50°

Fig. 3 Evolution of vortex structures during the downstroke of the flapping cycle for Case I-W and Case I at f =1.5 Hz (vorticity- line contour and λ_2 criterion- flood contour) (continued)

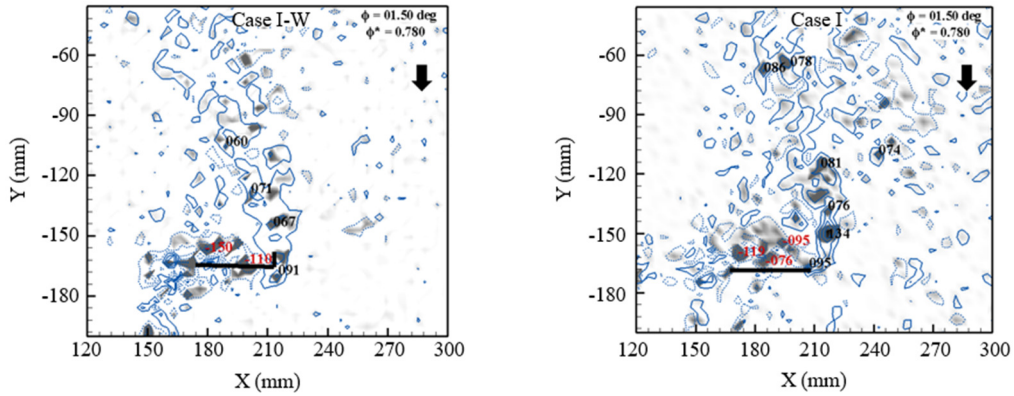

(i) Case I-W and Case I at ϕ = 01.50°

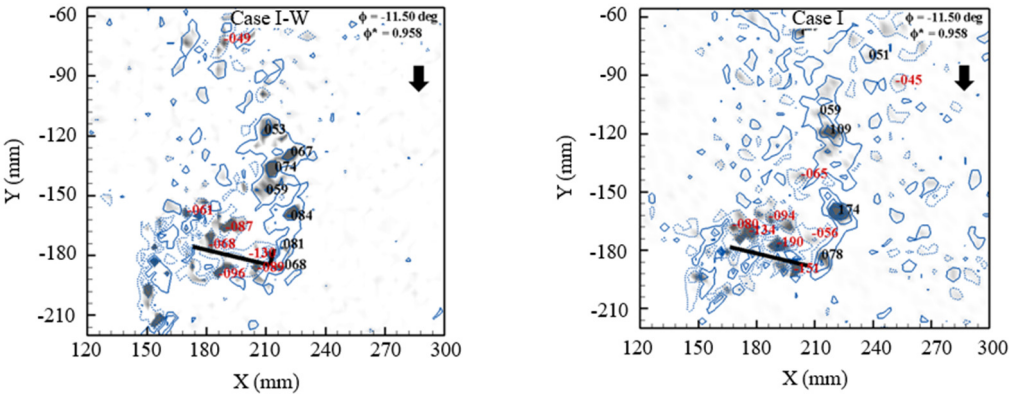

(j) Case I-W and Case I at ϕ = -11.50°

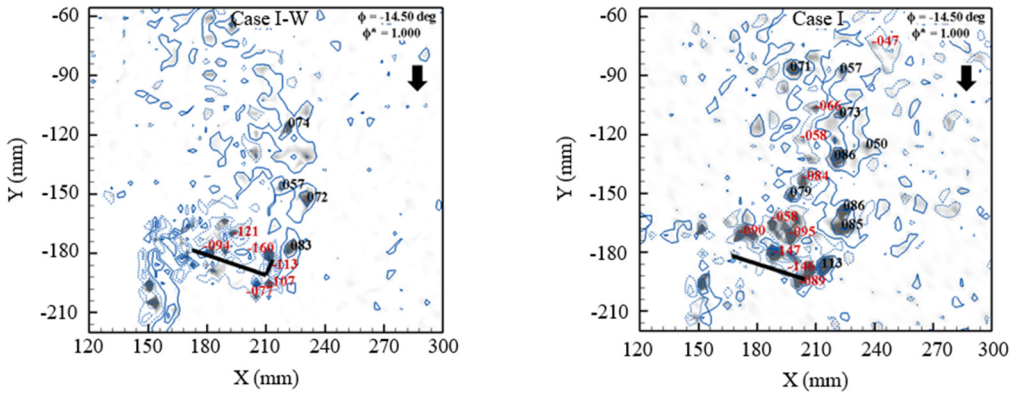

(k) Case I-W and Case I at ϕ = -14.50°

Fig. 3 Evolution of vortex structures during the downstroke of the flapping cycle for Case I-W and Case I at f =1.5 Hz (vorticity- line contour and λ_2 criterion- flood contour) (continued)

Vorticity is defined as ω_Z clockwise (CW) vorticity, $\omega_Z < 0$ has been represented by dotted contours, whereas counter-clockwise (CCW) vorticity, $\omega_Z > 0$ has been represented by continuous contours.

$$\omega_Z = \frac{\partial v}{\partial x} - \frac{\partial u}{\partial y} \tag{1}$$

The Galilean invariant vortex identification method proposed by Jeong and Hussain [25] is referred to as the λ_2 criterion. Swirling and shearing regions of the flow are correspondingly represented by negative and positive values of λ_2. Dark color denotes swirling regions, while white color signifies shearing regions. Regarding the present calculation, it used the equation for λ_2 reported by Goli et al. [26-27] and Vollmers [28].

$$\lambda_2 = \left(\frac{\partial u}{\partial x} + \frac{\partial v}{\partial y}\right)^2 - 4\left(\frac{\partial u}{\partial x} \times \frac{\partial v}{\partial y} + \frac{\partial u}{\partial y}\frac{\partial v}{\partial x}\right) \tag{2}$$

In the present section, the formation of wingtip vortices, counter-signed vortices due to residual flow (FACW, FACCW), and bound vortex has been observed. The comparison of the wing with a winglet and without a winglet has been discussed to understand the effect of a winglet attached to the wing.

A weak generation of wing-tip vortex (WTV1), characterized by a CCW nature, is observed close to the winglet during the initiation of the downstroke at $\phi = 58.50°$ (Fig. 3(a)). In the absence of winglets, a distinct WTV1 is observed near the wingtip. The bound vortices of both CCW and CW types can be observed on both the lower and upper surfaces of the wing in both scenarios. The lower surface bound vortex exhibits noticeably greater strength compared to the upper surface bound vortex. A CW vortex is observed to the right of the wingtip, at approximately one unit span distance for the winglet case and about two unit span distances for the case without winglets. This CW vortex has a lower magnitude than WTV1 in both cases. Henceforth it is referred to as the "far away CW vortex (FACW)."

Subsequently, the orientation of the FACW is nearly horizontal in the presence of winglets, while in the absence of winglets, it is approximately 20° below the horizontal. Simultaneously, vortices are also evident at the wing root, whereas they are not particularly strong. As the wing moves, an increase in size is observed in the WTV1, while a decrease in strength is observed. The lower surface of the wing witnesses the stretching out of the bound vortex towards the wing tip, resulting in a loss of strength, yet keeps feeding the WTV1. Likewise, the FACW vortex located to the right of the wing tip experiences an increase in size but a decrease in strength.

At $\phi = 55.50°$, $\phi = 53.50°$ (Fig. 3(b)-(c)), merging of the CCW bound vortex with the WTV1 enables it to augment in size and strength. For the winglet case, some part of WTV1 is found to have crossed the winglet. Furthermore, it is visible above the wing and close to the wingtip. Concerning the case without a winglet, the WTV1 is found to have grown in size and strength. CCW-bound vortex has moved towards the wingtip for both cases. For the winglet case, it is found to be distributed from mid-span to tip, while for the without winglet case, it is found to be distributed fully from root to tip. FACW moves along the vertical direction for both cases.

As the wing reaches $\phi = 47.50°$ (Fig. 3(d)), CCW bound vortex moves to the wingtip and feeds WTV1 which grows in size. For the winglet case, WTV1 is mostly outside the wing and located beside the winglet. It was observed from the beginning of the downstroke, that such phenomenon can be attributed to two reasons, i.e., the winglet acts as a fence, and only a limited portion of WTV1 rolls over the tip of the winglet to reach the upper surface of the wing. For without winglet case, WTV1 is observed to be deviating from the wingtip and appears to be getting detached from the wing. Meanwhile, the CW-bound vortex above the wing is found to have grown in size and has nearly covered the full span of the wing in both cases. FACW is found to be moving in a nearly vertical direction for both cases. Regarding the winglet case, it seems that WTV1 and FACW are close to each other and have strong interaction. Nevertheless, FACW breaks into fragments in the case without a winglet.

From $\phi = 47.50°$ to $\phi = 41.50°$ (Figs. 3(d)-(f)), the WTV1 grows like a balloon in both the cases. For the winglet case, as observed from the beginning of the stroke, WTV1 is located on the outer side of the winglet. Without a winglet case, it rolls over the upper side of the wing. In both cases, CCW-bound vortex is observed only at the wingtip, while the counterpart CW-bound vortex is fully developed and covers the wing from root to tip. FACW for the winglet case is near the WTV1. In the case of an absent winglet, it fragments further.

When the wing reaches $\phi = 22.50°$ (Figs. 3(f)-(h)), WTV1 and CCW bound vortex structures grow in size. These structures are nearly identical for both cases. The only difference is that the FACW still exists in the periphery of the winglet. Conversely, as observed from the beginning of the downstroke, it greatly deviates from the wingtip when the winglet is absent.

As the wing reaches $\phi = 01.50°$ (Fig. 3(i)), merely a negligible difference is observed between the two cases in the formation and appearance of vortex structures except the weak and small vortices formed in the far-field in the case of without winglet. The WTV1 grows like a vortex sheet along the locus of the wingtip. In this phase angle range, the dominant structures

are this vortex sheet and CW bound vortex, and these two features keep growing. In both cases, from ϕ = 01.50° to the end of the stroke ϕ = -14.50° (Figs. 3(i)-(k)), the vortex sheet and CW bound vortex keep growing in size, and it observed that vortex sheet tends to move out from the wing circumference as the wing reaches the end of the stroke due to the inclination caused by the wing sweeping to negative ϕ values.

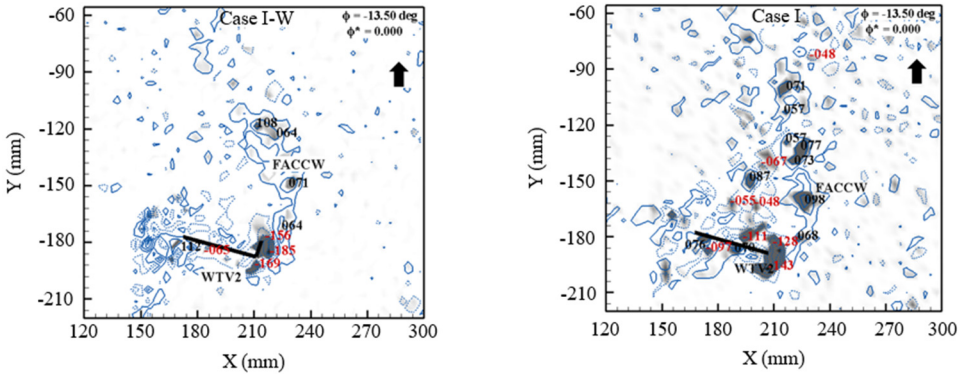

(a) Case I-W and Case I at ϕ = -13.50°

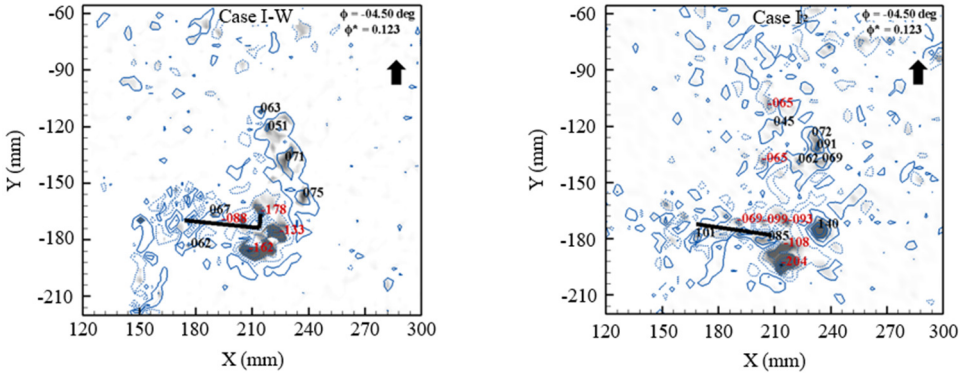

(b) Case I-W and Case I at ϕ = -04.50°

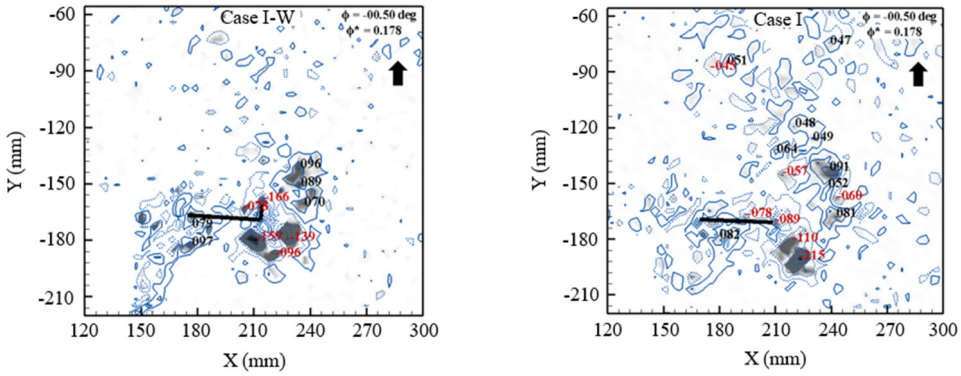

(c) Case I-W and Case I at ϕ = -00.50°

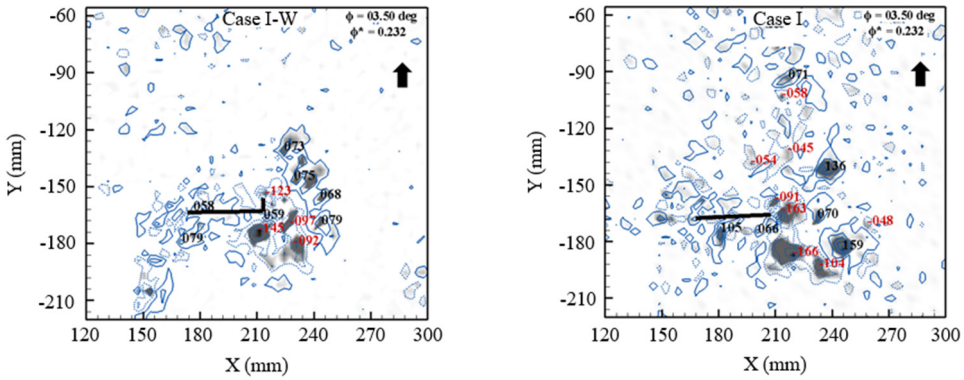

(d) Case I-W and Case I at ϕ = 03.50°

Fig. 4 Evolution of vortex structures during the upstroke of a flapping cycle for Case I-W and Case I at f =1.5 Hz (vorticity- line contour and λ_2 criterion- flood contour)

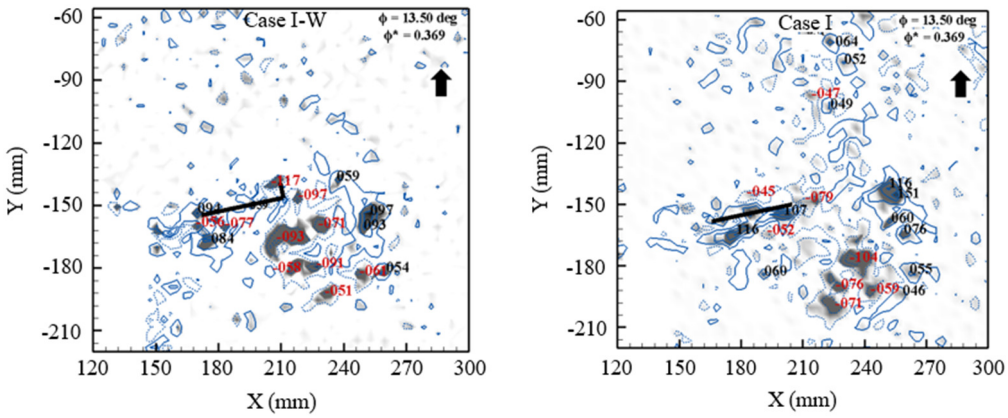

(e) Case I-W and Case I at ϕ = 13.50°

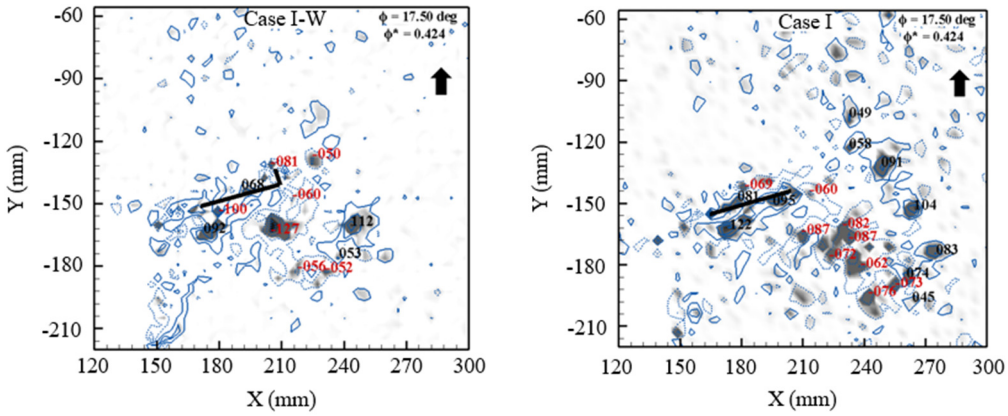

(f) Case I-W and Case I at ϕ = 17.50°

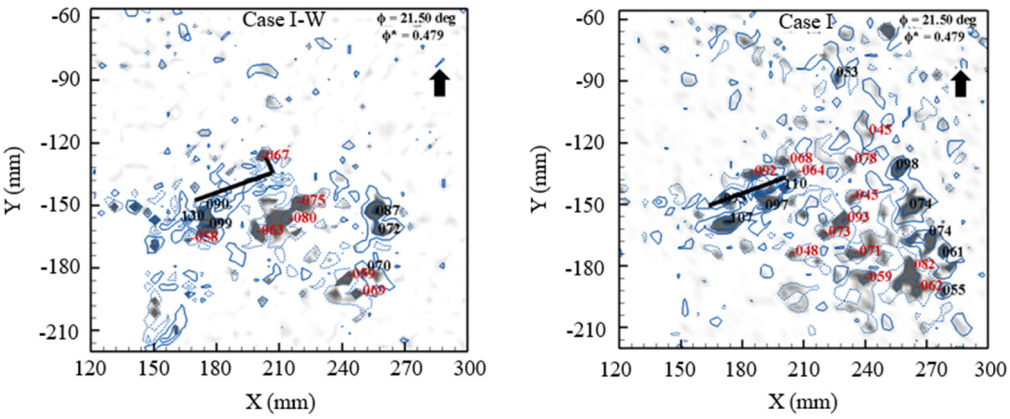

(g) Case I-W and Case I at ϕ = 21.50°

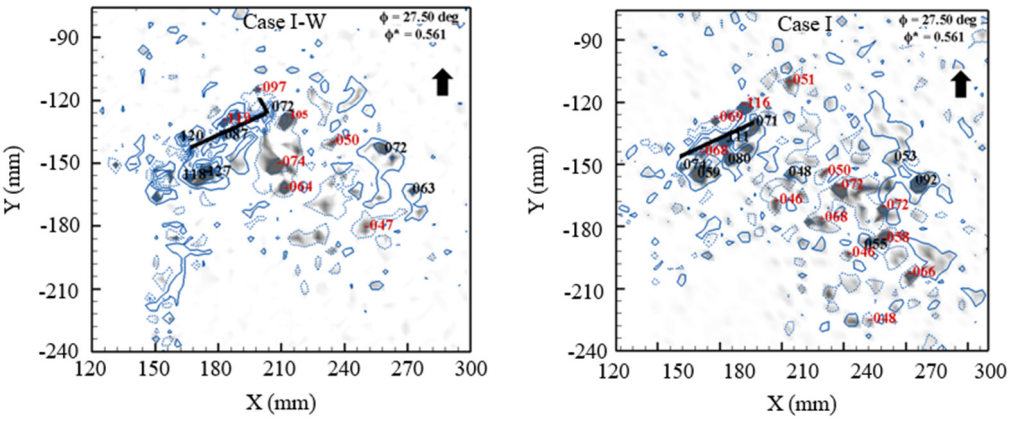

(h) Case I-W and Case I at ϕ = 27.50°

Fig. 4 Evolution of vortex structures during the upstroke of a flapping cycle for Case I-W and Case I at f =1.5 Hz (vorticity- line contour and λ_2 criterion- flood contour) (continued)

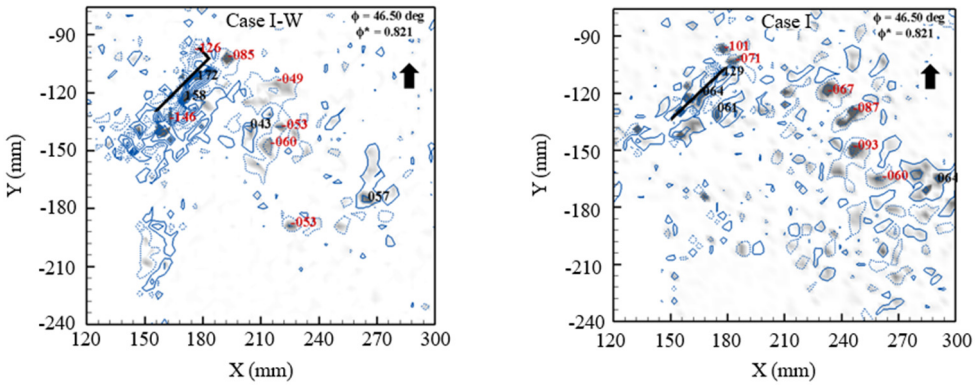

(i) Case I-W and Case I at ϕ = 46.50°

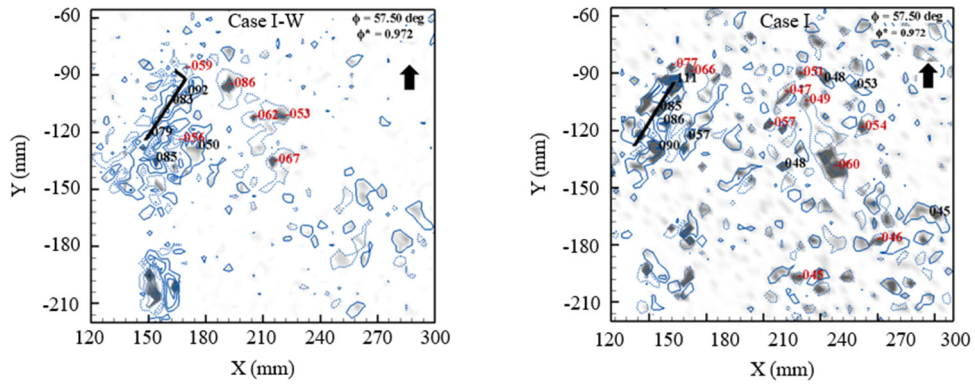

(j) Case I-W and Case I at ϕ = 57.50°

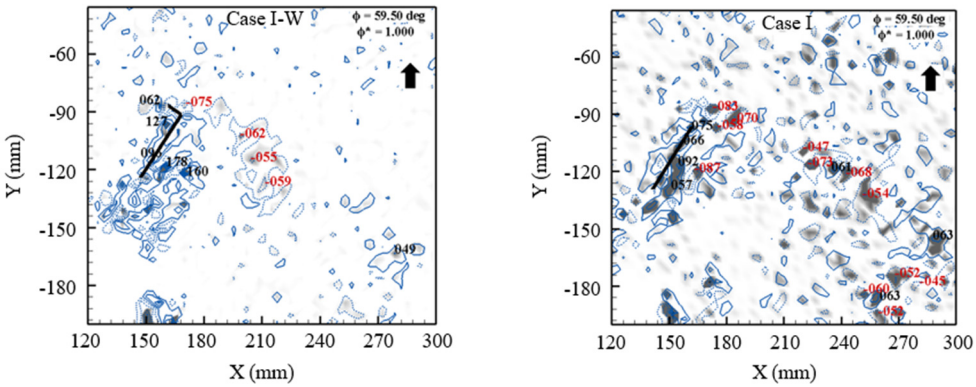

(k) Case I-W and Case I at ϕ = 59.50°

Fig. 4 Evolution of vortex structures during the upstroke of a flapping cycle for Case I-W and Case I at f =1.5 Hz (vorticity- line contour and λ_2 criterion- flood contour) (continued)

Given the results from Fig. 4 at the beginning of upstroke ϕ = -13.50° (Fig. 4(a)), CW wingtip vortex WTV2 formation is observed in both cases. A Bound vortex of CW nature is visible in both cases formed predominantly on the upper surface of the wing covering approximately three-fourth of the wingspan. Residual CCW vortices (FACCW) emerge as a sheet in the neighborhood of WTV2. The bound CCW vortex starts to grow on the upper surface of the wing near the wing root. The WTV2 for winglet case has higher strength in comparison with without winglet case.

At ϕ = -04.50° (Fig. 4(b)), the WTV2 grows in size in both the cases. For winglet case, is bigger than that without the winglet case. FACCW vortices are found to be moving down and away from the wing and oriented in a nearly horizontal direction. Bound vortex grows on the lower surface of the wing in either case.

When the wing reaches ϕ = 03.50° (Figs. 4(c)-(d)), the WTV2 grows in size and is found to be losing its strength. FACCW vortices of opposite signs are found beside it. For the winglet case, WTV2 is found to be lying closer to the wing. Bound vortex grows in size for either case. As the wing moves, WTV2 grows and spreads like a sheet in either case, and FACCW vortices still exist and interact with it. Bound vortex grows to occupy the full span of the wing.

At ϕ = 21.50° (Figs. 4(e)-(g)), WTV2 grows and breaks into smaller fragments due to a strong interaction with the opposite signed residual vortices FACCW and the subsequent movement deviating from the wing for both the cases. For the winglet case, WTV2 is more robust than without the winglet case. The bound vortex located on the lower surface of the wing continues to gain strength.

As the wing moves to ϕ = 27.50° (Fig. 4(h)), fragmented vortices move further away from the wing. From ϕ = 27.50° to the end of the stoke ϕ = 59.50° (Figs. 4(h)-(k)), a major portion of WTV2 disintegrates and continues to move in the upward direction. These fragmented vortices remain close to the wingtip approximately at a distance of unit span for the winglet case. Without a winglet case, the scattered vortex structures break further and continue to move upwards and further away from the wingtip. They are visible nearly at a distance of two times the wingspan. It is noteworthy that these vortices appear as FACW in the subsequent downstroke. In both cases, the bound vortex grows stronger and appears to be a dominant flow structure surrounding the wing.

3.2. Comparison of flow field behavior

When comparing between Case I-W and Case II-W without winglet [9] based on velocity field and vorticity with λ_2 criterion, the flow features are found to be predominantly similar. The dissimilarities are observed in the added mass, effective velocities, and vorticity magnitudes found to be higher in higher frequency cases. When comparing a wing with a winglet to a wing without a winglet, the major dissimilarities can be observed as follows.

(1) In the winglet cases, the formation of the wingtip vortex is not evident at the beginning of the downstroke. However, a stable shear layer is formed from the tip of the winglet. The evolution of the wingtip vortex during the downstroke and upstroke differs between the presence and absence of a winglet.

(2) The winglet case exhibits lesser added mass compared to the case without a winglet owing to entrainment reduction carried out by the shear layer originating from the tip of the winglet during the downstroke and from the wingtip corner, thereby impeding the growth of the added mass.

(3) In the winglet case, the formation of the residual vortex structure (FACW) occurs near the wingtip, at a radial distance approximately equal to the unit span level. In contrast, in the absence of the winglet, the residual vortex structure is located at a radial distance twice the span, with an angular orientation of approximately 20 degrees downwards relative to the level of the wingtip.

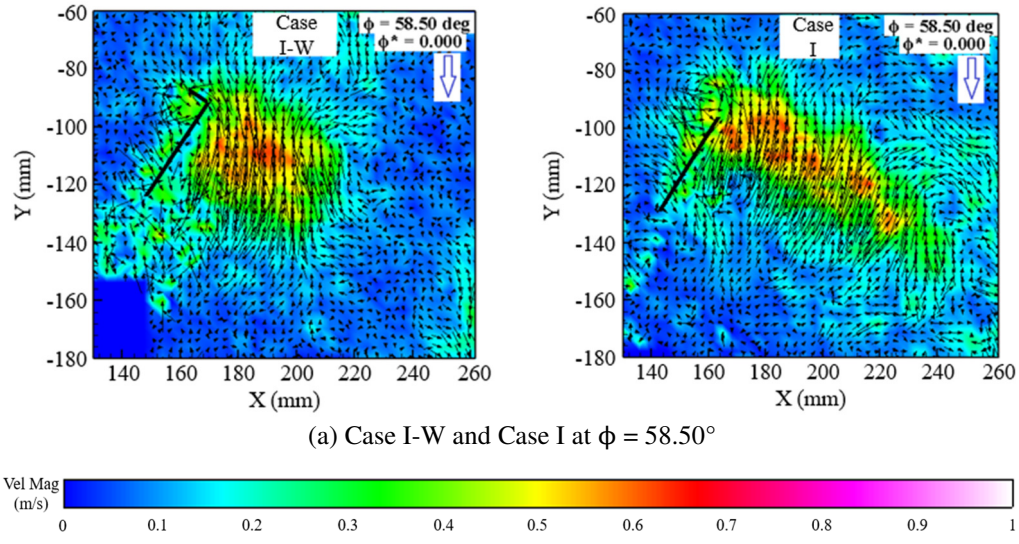

(a) Case I-W and Case I at ϕ = 58.50°

Fig. 5 Comparison of the velocity field at the beginning of the downstroke

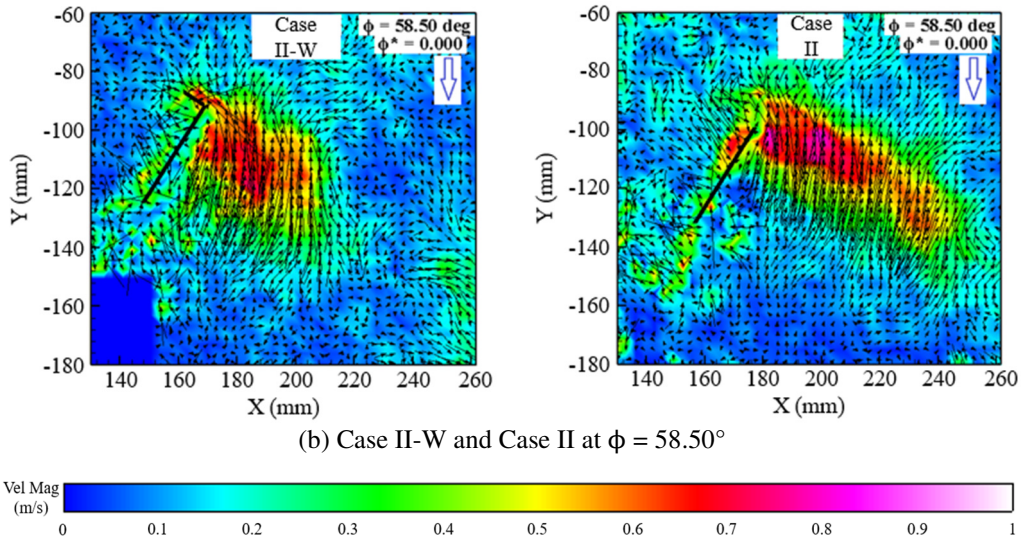

(b) Case II-W and Case II at ϕ = 58.50°

Fig. 5 Comparison of the velocity field at the beginning of the downstroke (continued)

The comparison of the wing with a winglet and the wing without a winglet at the beginning of the downstroke and upstroke is shown in Figs. 5 to 8. The velocity field is depicted in Figs. 5 and 6, while Figs. 7 and 8 present the vorticity with the λ_2 criterion. It is evident from the figures that the winglet functions as a fence or a one-sided splitter plate. The flow field in its immediate neighborhood is significantly influenced by the winglet, and it also affects the evolution of the overall flow field structures during wing flapping.

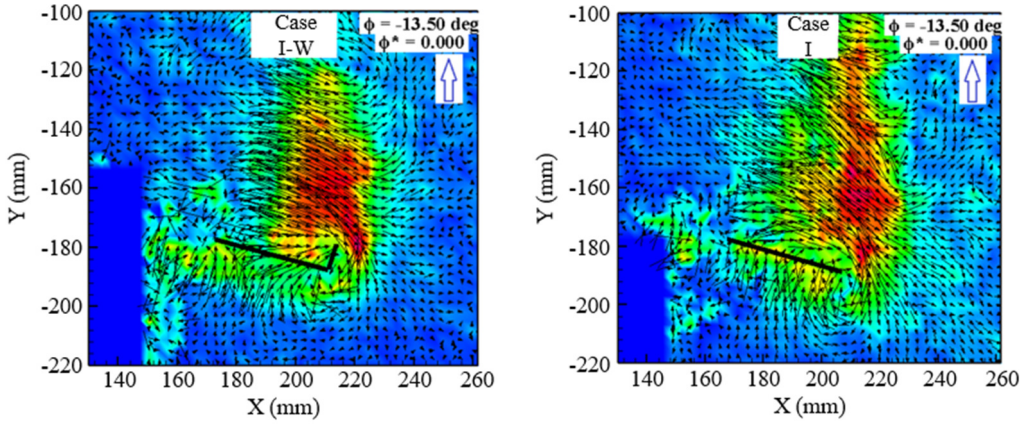

(a) Case I-W and Case I at ϕ = -13.50°

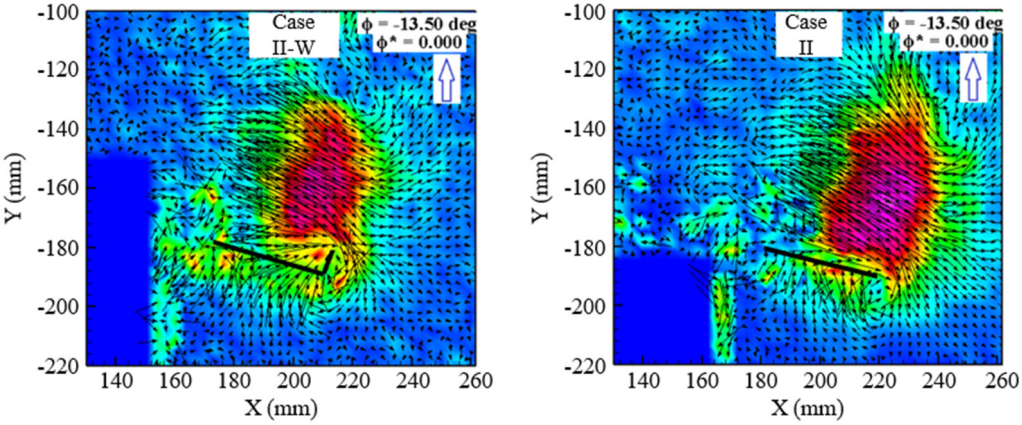

(b) Case II-W and Case II at ϕ = -13.50°

Fig. 6 Comparison of the velocity field at the beginning of the upstroke

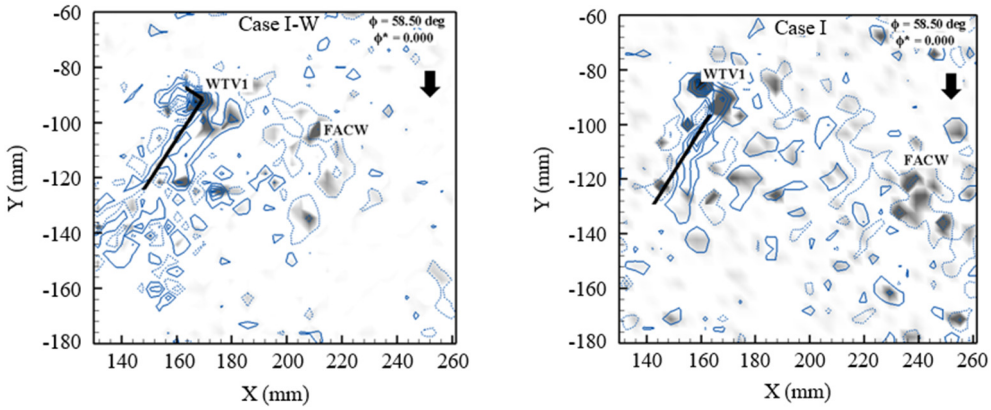

(a) Case I-W and Case I at ϕ = 58.50°

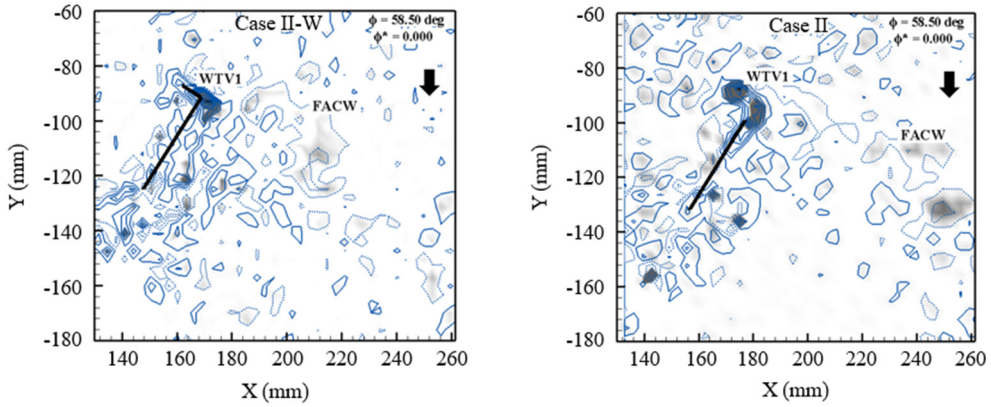

(b) Case II-W and Case II at ϕ = 58.50°

Fig. 7 Comparison of vorticity with λ_2 criterion at the beginning of the downstroke

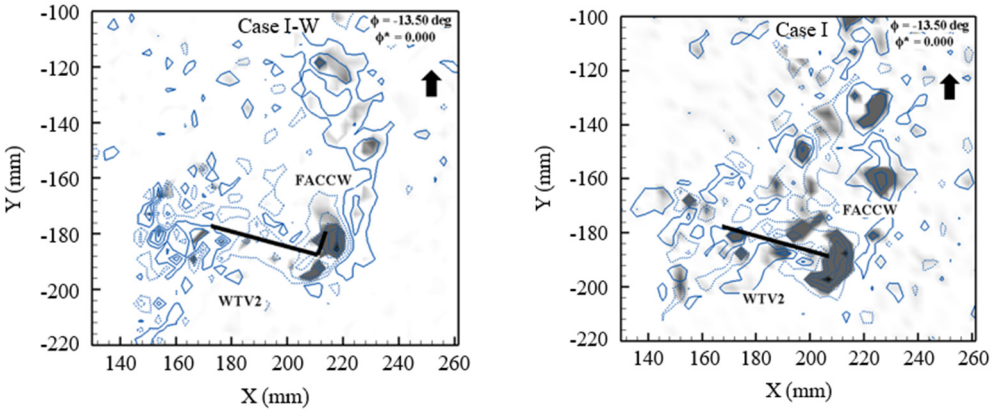

(a) Case I-W and Case I at ϕ = -13.50°

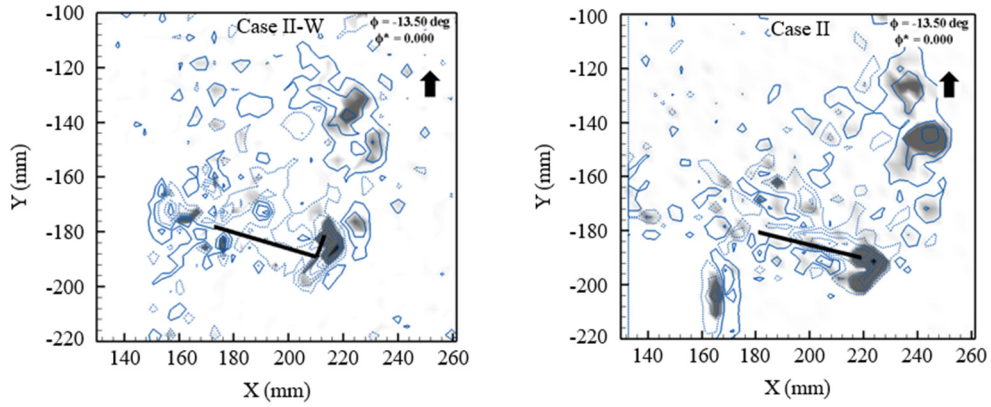

(b) Case II-W and Case II at ϕ = -13.50°

Fig. 8 Comparison of vorticity with λ_2 criterion at the beginning of the upstroke

To achieve brevity, the detailed figures corresponding to Cases II-W and II are not included herein. To provide a generic representation of the flow features during the downstroke and upstroke, schematic diagrams are presented in Figs. 9 and 10, which illustrate the cases with a winglet and without a winglet, respectively.

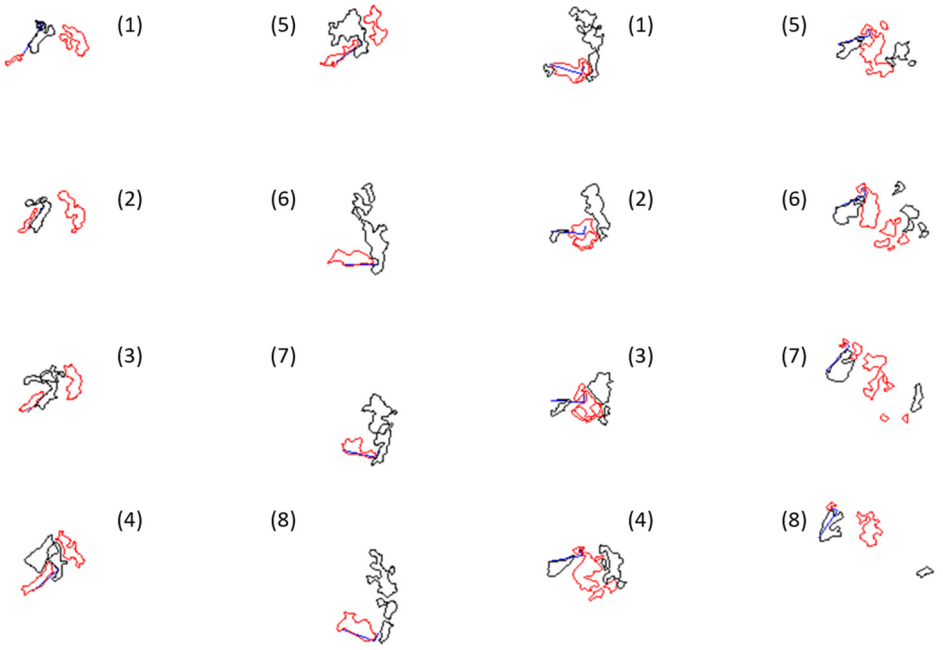

(a) Downstroke (b) Upstroke

Fig. 9 Schematic of vortex structures during downstroke and upstroke in the flapping cycle: wing with a winglet Case I-W and Case II-W

*Red and black color indicates clockwise and counter-clockwise directions, respectively.

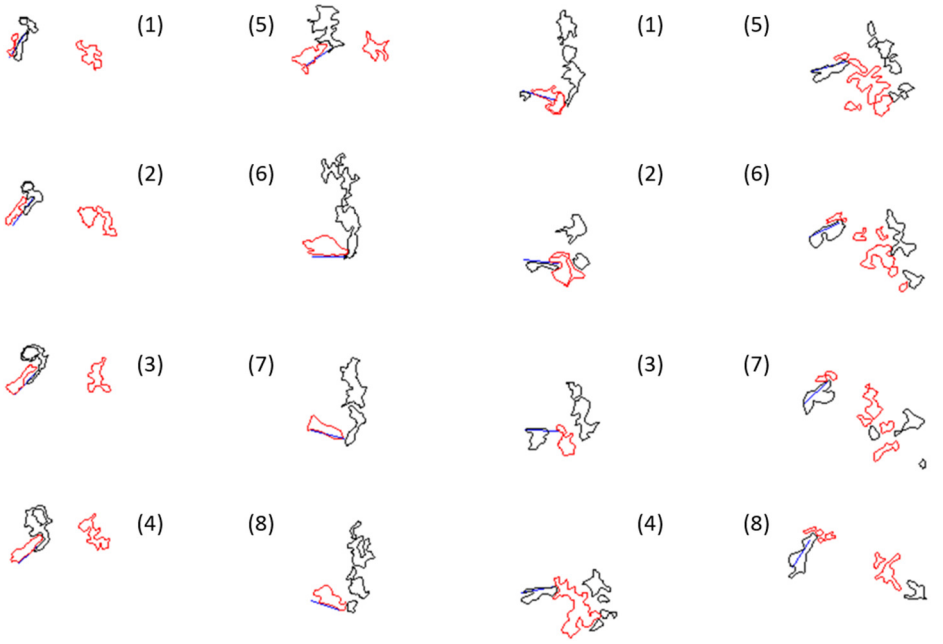

(a) Downstroke (b) Upstroke

Fig. 10 Schematic of vortex structures during downstroke and upstroke in the flapping cycle: wing without a winglet Case I and Case II

*Red and black color indicates clockwise and counter-clockwise directions, respectively.

Vortex filamentation and fragmentation have been reported during the downstroke and upstroke, respectively, based on the observed flow field features in Goli et al. [17, 22]. A “modified” vortex filamentation and fragmentation are observed during the downstroke and upstroke, respectively, in the winglet study conducted at two frequencies (Cases I-W and II-W).

The term “modified” is used to highlight the dissimilar formation of the wingtip vortex in the early part of the strokes and the presence of a strong shear layer originating from the winglet or wingtip. The remaining flow features that define the phenomena remain consistent when the winglet is present.

4. Conclusions

A corollary has been proposed as “modified” vortex filamentation and fragmentation phenomena during downstroke and upstroke respectively for a rigid flapping wing with a winglet based on the hypothesis reported in Goli et al. [17, 22] for the study without a winglet. The wing formation and growth of added mass the suction side were found to be profoundly influenced by the presence or absence of a winglet. The suction is created by the movement of the wing, while the winglet functions as a fence or barrier for the nearby flow. Regarding the winglet, a strong wingtip flow is generated by the residual flow during the downstroke, which energizes a shear layer formed at the tip of the winglet.

This shear layer reduces entrainment and consequently inhibits the growth of the added mass. Conversely, Concerning the absence of a winglet, the residual flow upon crossing the wingtip tends to move further away from it, allowing significant entrainment and growth of the added mass as it mixes with the neighboring flow along the wingtip’s path. Therefore, a strong interaction of the residual flow reduces the added mass in the winglet case, while a weak interaction enhances the added mass when the winglet is absent. Similar behavior is observed during the upstroke, resulting in reduced formation of added mass in the winglet case.

Practical applications can be derived from the results of the current work with an expected generation of an upward force through the proposed corollary. Consequently, the study’s findings can be deployed in the design of vehicles for missions that primarily necessitate upward movement. The future research scope encompasses the assessment of performance through force/moment measurements, power requirements, execution of comprehensive parametric investigations, and the conduct of airborne tests. Moreover, with a specific emphasis on the tracing of the evolutionary cycle of certain vortex forms, valuable insights may be gained from further investigation of the unsteady flow field surrounding a flapping wing, performing CFD simulations and POD techniques.

Acknowledgment

The authors would like to thank KFUPM for the research support. This research was funded through projects sponsored by the following agencies: (i) the Aeronautics R&D Board, Government of India (sanction letter no. ARDB/01/1031864/M/I), and (ii) the Department of Science and Technology, Government of India [sanction letter no. SR/FST/ETI-386/2014 (G)].

Conflicts of Interest

The authors declare no conflict of interest.

References

[1] R. T. Whitcomb, “A Design Approach and Selected Wind Tunnel Results at High Subsonic Speeds for Wing-Tip Mounted Winglets,” NASA Langley Research Center Hampton, VA, Technical Report NASA-TN-D-8260, July 01, 1976.

[2] S. G. Flechner, P. F. Jacobs, and R. T. Whitcomb, “A High Subsonic Speed Wind Tunnel Investigation of Winglets on a Representative Second-Generation Jet Transport Wing,” NASA Langley Research Center Hampton, VA, Technical Report NASA-TN-D-8264, July 01, 1976.

[3] I. Kroo, “Drag Due to Lift: Concepts for Prediction and Reduction,” Annual Review of Fluid Mechanics, vol. 33, pp. 587-617, January 2001.

[4] J. R. Spreiter and A. H. Sacks, “The Rolling Up of the Trailing Vortex Sheet and Its Effect on the Downwash Behind Wings,” Journal of the Aeronautical Sciences, vol. 18, no. 1, pp. 21-32, January 1951.

[5] M. Berens, "Potential of Multi-Winglet Systems to Improve Aircraft Performance," Ph.D. dissertation, Technical University of Berlin, Germany, 2008.
[6] G. Srikanth and B. Surendra, "Experimental Investigation on the Effect of Multi-Winglets," International Journal of Mechanical and Industrial Engineering, vol. 1, no. 1, pp. 43-46, 2011.
[7] G. Narayan and B. John, "Effect of Winglets Induced Tip Vortex Structure on the Performance of Subsonic Wings," Aerospace Science and Technology, vol. 58, pp. 328-340, November 2016.
[8] M. Smith, N. Komerath, R. Ames, O. Wong, and J. Pearson, "Performance Analysis of a Wing with Multiple Winglets," 19th AIAA Applied Aerodynamics Conference, article no. 2407, June 2001.
[9] S. Goli, A. Roy, and S. Roy, "Velocity Field around a Rigid Flapping Wing with a Winglet in Quiescent Water," Advances in Technology Innovation, vol. 5, no. 4, pp. 259-269, October 2020.
[10] V. A. Tucker, "Gliding Birds: Reduction of Induced Drag by Wing Tip Slots Between the Primary Feathers," Journal of Experimental Biology, vol. 180, no. 1, pp. 285-310, July 1993.
[11] S. Goli, A. Roy, D. K. Patel, and S. Roy, "Particle Image Velocimetry Measurements of Rigid and Flexible Rectangular Wings Undergoing Main Flapping Motion in Hovering Flight," Fluid Mechanics and Fluid Power – Contemporary Research: 5th International and 41st National Conference on FMFP 2014, pp. 1411-1420, 2017.
[12] Y. S. Hong and A. Altman, "Lift from Spanwise Flow in Simple Flapping Wings," Journal of Aircraft, vol. 45, no. 4, pp. 1206-1216, July-August 2008.
[13] H. Hu, A. G. Kumar, G. Abate, and R. Albertani, "An Experimental Investigation on the Aerodynamic Performances of Flexible Membrane Wings in Flapping Flight," Aerospace Science and Technology, vol. 14, no. 8, pp. 575-586, December 2010.
[14] K. Mazaheri and A. Ebrahimi, "Experimental Study on Interaction of Aerodynamics with Flexible Wings of Flapping Vehicles in Hovering and Cruise Flight," Archive of Applied Mechanics, vol. 80, no. 11, pp. 1255-1269, November 2010.
[15] K. Mazaheri and A. Ebrahimi, "Experimental Investigation of the Effect of Chordwise Flexibility on the Aerodynamics of Flapping Wings in Hovering Flight," Journal of Fluids and Structures, vol. 26, no. 4, pp. 544-558, May 2010.
[16] N. Kato and S. Kamimura, Bio-Mechanisms of Swimming and Flying: Fluid Dynamics, Biomimetic Robots, and Sports Science, Berlin: Springer, 2008.
[17] S. Goli, A. Roy, and S. Roy, "Vortex Filamentation and Fragmentation Phenomena in Flapping Motion and Effect of Aspect Ratio and Frequency on Global Strain, Rotation, and Enstrophy," International Journal of Micro Air Vehicles, vol. 11, pp. 1-30, January-December 2019.
[18] F. Centracchio, M. Rossetti, and U. Iemma, "Approach to the Weight Estimation in the Conceptual Design of Hybrid-Electric-Powered Unconventional Regional Aircraft," Journal of Advanced Transportation, vol. 2018, article no. 6320197, 2018.
[19] R. R. Mouliswar, K. Chandrasekaran, T. Ranganathan, and A. Thondiyath, "Computational Fluid Dynamic Study on the Effect of Winglet Addition in Flapping Hydrofoils to Evaluate the Propulsive Performance of Wave Gliders," Oceans 2022 - Chennai, pp. 1-4, February 2022.
[20] D. Samanta and R. Kumar, "Numerical Simulation of Flexible and Shape Morphing Flapping Wing Using Discrete Vortex Method," SSRN, in press. http://dx.doi.org/10.2139/ssrn.4194408
[21] S. Qin, Z. Weng, Z. Li, Y. Xiang, and H. Liu, "On the Controlled Evolution for Wingtip Vortices of a Flapping Wing Model at Bird Scale," Aerospace Science and Technology, vol. 110, article no. 106460, March 2021.
[22] S. Goli, A. Roy, and S. Roy, "Effect of Marginal Variation of Aspect Ratio and Frequency with Kinematic Asymmetry on Flow Field Around Flapping Rigid Wing in Hover," Results in Engineering, vol. 18, article no. 101199, June 2023.
[23] W. Yamazaki and H. Yamada, "PIV Data Analysis around a Flapping Wing via Proper Orthogonal Decomposition," 43rd Fluid Dynamics Conference, article no. 2473, June 2013.
[24] C. A. Ozen and D. Rockwell, "Vortical Structures on a Flapping Wing," Experiments in Fluids, vol. 50, no. 1, pp. 23-34, January 2011.
[25] J. Jeong and F. Hussain, "On the Identification of a Vortex," Journal of Fluid Mechanics, vol. 285, pp. 69-94, February 1995.
[26] S. Goli, S. S. Dammati, A. Roy, and S. Roy, "Coherent Structures in the Flow Field Generated by Rigid Flapping Wing in Hovering Flight Mode," IOP Conference Series: Materials Science and Engineering, vol. 402, article no. 012155, 2018.
[27] S. Goli, S. S. Dammati, A. Roy, and S. Roy, "Vortex Identification and Proper Orthogonal Decomposition of Rigid Flapping Wing," International Journal of Fluid Mechanics Research, vol. 47, no. 4, pp. 309-328, 2020.
[28] H. Vollmers, "Detection of Vortices and Quantitative Evaluation of Their Main Parameters from Experimental Velocity Data," Measurement Science and Technology, vol. 12, no. 8, article no. 1199, August 2011.